Time Stretching of the GeV Emission of GRBs: Fermi LAT data vs geometrical model

Maxim S. Piskunov[1]*and Grigory I. Rubtsov[1]†
[1]Institute for Nuclear Research RAS, 117312, Moscow, Russia

March 23, 2014

Abstract

Numerous observations confirm that the high energy ($> 100\,\mathrm{MeV}$) emission of gamma ray bursts is delayed with respect to the low energy emission. However, the difference of light curves in various high energy bands has not been studied properly.

In this paper we consider all the bursts observed by Fermi-LAT since 2008 August 4 to 2011 August 1, for which at least 10 events with energies 1 GeV or higher were observed. There are 4 of them: 080916C, 090510, 090902B, and 090926A. We study their light curves in two bands, $(100\,\mathrm{MeV}, 1\,\mathrm{GeV})$ and $(1\,\mathrm{GeV}, 300\,\mathrm{GeV})$. The Kolmogorov-Smirnov test is used to check whether the light curves for these two bands are the same. No significant difference was found for 080916C and 090510. However, we observed with statistical significance of 3.3σ, that the higher energy light curve of 090926A is stretched with respect to the lower-energy one, and with statistical significance of 2.2σ, that the lower energy light curve of 090902B is stretched with respect to the higher-energy one.

We suggest a simple geometrical model to explain this result. The main assumption is the jet opening angle dependence on radiation energy – the most energetic photons are emitted near the axis of the jet. To test this model, we compute the total energy of the burst, and confirm that it is below the constraint. We also compute the fraction of observable bursts in $(100\,\mathrm{MeV}, 1\,\mathrm{GeV})$ band, which can also be observed in higher energies. This fraction matches the observations. Finally, we predict the distribution of observable stretching factors, which may be tested in the future when more observational data will be available.

1 Introduction

Gamma Ray Bursts (GRBs) are among the most energetic events in the Universe, therefore they might provide new knowledge for particle physics. Modern observatories, specifically Fermi [Fermi-LAT12] and Swift [Science04] made possible to study these explosions extensively [Via13, GR13]. These and previous studies led to several interesting results. For example, the total energy emitted in gamma-rays during a burst was found to be similar among different bursts within an order of magnitude [BFK03]. This suggests that most of the bursts must have similar energetics in their rest frame. Temporal variations of spectra were also studied. The spectral lags were found between different low energy bands [YLQL06]. The very high energy radiation was discovered to be extended relative to x-ray emission [Via13, LP13]. Moreover, the Large Area Telescope (LAT) of Fermi allows us to explore the spectral variations even between high energy bands like $(100\,\mathrm{MeV}, 1\,\mathrm{GeV})$ and $(1\,\mathrm{GeV}, 300\,\mathrm{GeV})$ (we call them low and high energy bands throughout the paper). In this study we use the Kolmogorov-Smirnov test to compute the time stretching of radiation in one of these bands compared to the other.

We take the GRB list from the Fermi-LAT catalog [AAA+13]. Tables 2 and 4 in [AAA+13] provide the time, durations and locations of the bursts, which we use to download observational data from the LAT

*maxit@ms2.inr.ac.ru
†grisha@ms2.inr.ac.ru

Data Server[1]. We also download events during a day before the burst, and use the technique introduced in [RPT12] to estimate background radiation in both energy bands. Most of the bursts in the catalog, however, do not have enough events with over 1 GeV energies to do desired computations, so we choose only those bursts, from which at least 10 photons were detected in the high energy band. This leaves 3 of them: 080916C [FLG09], 090902B [FS09] and 090926A [Fermi11].

For these 3 bursts we compute both high and low energy distributions of photon times. We subtract the low energy background estimate from the low energy CDF, and add the high energy background estimate to it. This makes the low energy CDF non-monotonous and, rigorously speaking, we cannot use the 2-sample Kolmogorov-Smirnov test on it. However, since there is a much greater number of photons on lower energies, we can think of the low energy CDF as continuous. Therefore, this non-monotonicity will be negligible, and will not harm the KS-test results much.

Finally, we stretch the high energy CDF by different factors, and compare it to the low energy CDF using the KS-test. If we require 2σ-significant probability to exclude a particular stretching factor, then the stretching factor of 1 (which means no stretching) is allowed for GRBs 080916C and 090902B. However, for 090926A, the stretching factor of 1 is prohibited, so the high energy light curve should be stretched with respect to the low energy one.

We propose that this result can be explained by the curvature effects (that is the effects of the jet geometry). These effects were explored by multiple authors [NI01, SSL05, SSD$^+$13]. However, these studies were only concerned with x-ray radiation, and, even more importantly, they assumed that the distribution of radiation sources is homogeneous throughout the jet. We propose a contrary idea: that the highest energy radiators are concentrated near the axis of the burst, meaning that the burst opening angle depends on energy. We cannot prove this assumption rigorously, but have arguments supporting it.

First of all, there are around 750 GRBs detected by GBM, half of which were in the LAT field of view at the moment of observation [Via13]. However, only about 30 of them were detected by the LAT, and only 3 of them were bright in the high energy band. If we extrapolate the uniform jet model to very high energies, this observation would mean that these groups of bursts are internally different: some of them produce VHE radiation, and other do not. These differences are hard to explain given that burst energetics are similar [BFK03]. Nevertheless, these differences in burst counts can easily be explained by our model. In our model, the opening angle of a jet is inversely proportional to the energy of photons it radiates. Therefore the most common scenario is that the off-axis angle of the observer is smaller than the low energy jet opening angle, but larger than the opening angle of a high energy jet. Because of that, most of the bursts can only be seen at low energies. The 3 bursts we study in this paper, were seen, according to our model, from the lowest off-axis angles.

Second, consider the plasma right after its ejection from the central engine. Two processes happen there simultaneously:

1. Particles near the jet boundary change their movement directions, therefore increasing the opening angle of the jet.

2. Particles lose energy, therefore decreasing radiation frequency emitted by the jet.

We argue that these two processes are correlated, for they happen due to the same particle interaction processes. And since they are correlated, jets with larger opening angles should have lower energies, which is the assumption we are trying to justify.

Finally, our assumption is able to explain the non-trivial stretching factor of both GRBs 090902B and 090926A. Detailed computations will be described in the following sections, but you can see the main idea on the figure 1. The computations confirm that this qualitative picture is indeed correct. You can see a sample light curves on the figure 2, and predicted distribution of stretching factors on the figure 7.

[1] `http://fermi.gsfc.nasa.gov/cgi-bin/ssc/LAT/LATDataQuery.cgi`

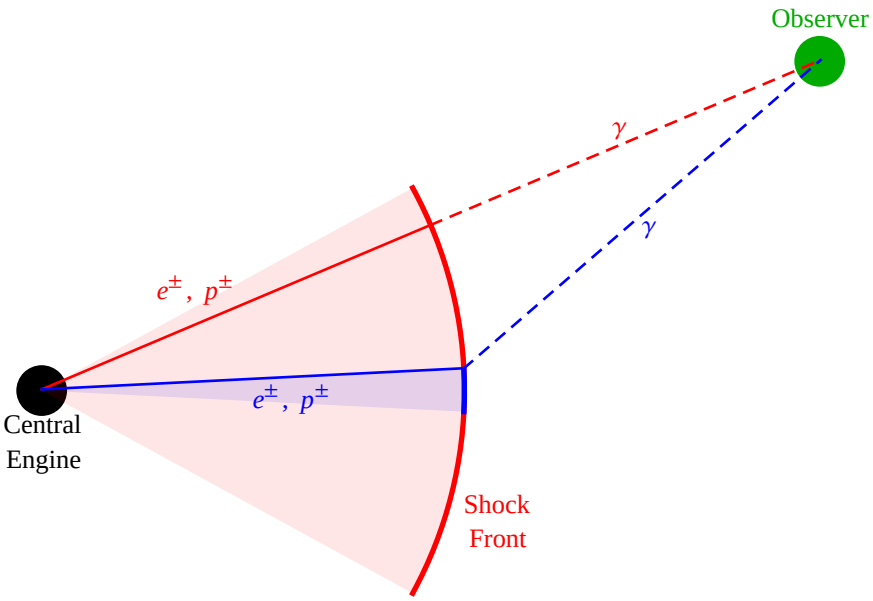

Figure 1: Model Overview. Here the red and the blue cones represent the volumes through which low and high energy plasma propagates. In case depicted the observer's off-axis angle is smaller than the opening angle of the low energy jet, so, due to the relativistic beaming effect, the most of the observable low energy photons will travel along the straight line from the central engine. Also, the observer's off-axis angle is larger that the opening angle of the high energy jet, so the high energy radiation will still originate near the center of the jet (because it is the only place where there are high energy radiators). The observation time of a photon is a sum of two things: the time interval spent in plasma as a radiator (which approximately equals to the distance from the central engine to the point of emission); and the time interval from emission to detection (which is the distance from the point of emission to the observer's location). Given a position of the shock front, this sum is larger for high energy photons. Because of that, high energy emission will be observed later throughout the burst duration, therefore the high energy light curve will be stretched.

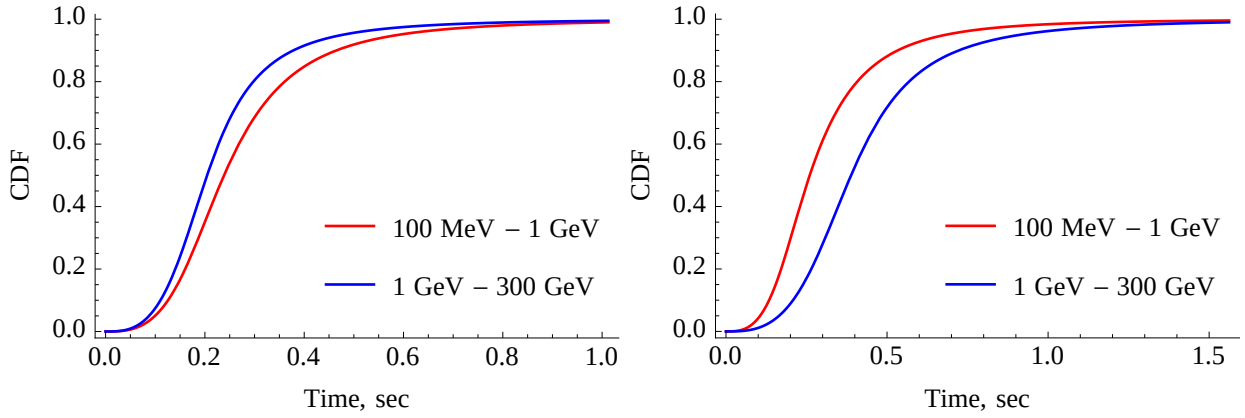

Figure 2: High and low energy light curves produced by the geometrical model. Parameter values are the same as discussed in the section 3.9. Redshift $z = 1$. Observer's off-axis angles are $\chi = 0$ for the left figure, and $\chi = 0.01$ for the right one.

`name`	`time`	`location.ra`	`location.dec`	`location.err`	`startOffset`	`endOffset`
GRB	GBM Trigger Time	R.A.	Dec.	Location Error	T_{05}	T_{95}
Name	MET, sec	J2000, deg	J2000, deg	deg	sec	sec
080825C	241 366 429.105	233.9	−4.5	0.75	3.2	29.4
080916C	243 216 766.614	119.85	−56.64	0.0001	5.0	209.8
081006	244 996 175.173	136.32	−62.05	0.52	0.7	115.0
081024B	246 576 161.864	322.95	21.2	0.22	0.1	191.0
090217	256 539 404.560	204.83	−8.42	0.35	6.2	68.0
090323	259 459 364.630	190.71	17.053	0.0001	15.9	293.9
090328	259 925 808.510	90.67	−41.715	0.0002	18.8	652.9
090510	263 607 781.971	333.55	−26.583	0.0004	0.6	45.6
090626	267 683 530.880	170.03	−33.49	0.22	52.2	299.9
090902B	273 582 310.313	264.94	27.324	0.001	7.7	825.0
090926A	275 631 628.990	353.4	−66.32	0.01	5.5	225.0
091003	276 237 347.585	251.52	36.625	0.0005	3.9	452.6
091031	278 683 230.850	71.49	−57.65	0.23	3.1	206.2
100116A	285 370 262.240	305.01	14.43	0.17	3.0	141.0
100414A	292 904 423.990	192.11	8.693	0.0005	17.4	288.6
110120A	317 231 981.230	61.5	−12.0	0.36	0.5	112.8
110428A	325 675 112.410	5.59	64.849	0.000 01	10.7	407.6
110721A	332 916 465.760	333.2	−38.5	0.20	0.1	239.0
110731A	333 803 371.954	280.504	−28.537	0.0001	3.0	24.1

Table 1: Burst data used in our study. The first row contains the corresponding `GRBurst` class variable names. The data is taken from the tables 2 and 4 of [AAA+13]. `https://github.com/maxitg/GammaRays/blob/master/GRObservations/bursts`

2 Observations

2.1 Burst Data Download

Before we start to compute the Kolmogorov-Smirnov probabilities, we need to download the actual observational data from the Fermi LAT data server. We take the data about the bursts from the catalog [AAA+13], which contains all the bright bursts seen by the LAT since 2008 August 4 to 2011 August 1. Specifically, we take 4 pieces of information from the tables 2 and 4 there:

- GBM trigger time (table 2). It is used as a reference point for the GRB time.
- Location of the GRB (table 2). We need burst locations to filter out photons coming from other sources.
- Location error (table 2). Location errors are used to improve accuracy of filtering, specifically to avoid losing statistics by filtering too much.
- T_{05} – T_{95} interval of the LAT-detected emission (table 4). We need precise intervals for two things. First, to understand where is the fixed point of the stretching (T_{05} is used as a proxy for that). Second, the burst interval is used to download events data from the data server.

The data obtained is summarized in the table 1.

Finally, to download the data about observed photons, we fill the form at the LAT data server front page with the following values:

- **Object name or coordinates**. Here the coordinates are filled from the table 1.
- **Coordinate system**. J2000.

- **Search radius (degrees)**. 60. Events will be filtered by location later on by using the point spread functions (PSFs) of the LAT.
- **Observation dates**. To have a decent safety margin, we extend the duration of the burst by 15% to both past and future relative to the table 1 time ranges. So, we fill in the following values:

$$\texttt{time} + \texttt{startOffset} - 0.15\,(\texttt{endOffset} - \texttt{startOffset})\,,$$
$$\texttt{time} + \texttt{endOffset} + 0.15\,(\texttt{endOffset} - \texttt{startOffset})$$

- **Time system**. MET.
- **Energy range (MeV)**. 30, 300000. The whole energy range is required for our study.
- **LAT data type**. Extended, because we need transient photons for better statistics.
- **Spacecraft data**. Checked. It is required for both events filtering, and calculation of the PSFs and exposure maps.

For background estimation, we also download observational data during a day before the burst. All the values are put the same into the form, except the time range:

$$\texttt{time} + \texttt{startOffset} - 0.15\,(\texttt{endOffset} - \texttt{startOffset}) - 86400\,\text{sec},$$
$$\texttt{time} + \texttt{startOffset} - 0.15\,(\texttt{endOffset} - \texttt{startOffset})$$

All other values filled in the form are the same.

Before reading the data, we need to apply the basic filtering as described in Fermi guidelines. Two tools from the Fermi Science Tools package are used for that task (the same filtering is applied to both burst and background data).

The first one is `gtselect`[2]. It filters the Earth limb emission. We run the tool with the following parameters[3]:

```
gtselect infile=[eventFile] outfile=filtered.fits
       ra=INDEF dec=INDEF rad=180 tmin=INDEF tmax=INDEF emin=100 emax=300000
       zmax=100 evclass=0 convtype=-1 evtable=EVENTS
```

Here `[eventFile]` is the file downloaded in the previous step.

The second one is `gtmktime`[4]. It uses the spacecraft file as well as events file, and filters out time periods when Fermi LAT was not operational. Running `gtmktime` is also required for exposure maps calculation, which we'll need later on. Parameters are the following[5]:

```
gtmktime scfile=[spacecraft] sctable=SC_DATA
       filter="DATA_QUAL>0 && LAT_CONFIG==1" roicut=yes
       evfile=filtered.fits evtable=EVENTS outfile=timed.fits
       apply_fiter=yes
```

where `[spacecraft]` is the FITS containing the spacecraft data.

Now, with basic filtering done, we can read events data from `timed.fits`. This file, however, contains observations of a large area of the sky. Before using the data obtained from it, we should perform a more elaborate filtering by location using Fermi LAT's point spread function, which will be described in the following section.

[2] `http://fermi.gsfc.nasa.gov/ssc/data/analysis/scitools/help/gtselect.txt`
[3] `http://fermi.gsfc.nasa.gov/ssc/data/analysis/scitools/explore_latdata_burst.html`
[4] `http://fermi.gsfc.nasa.gov/ssc/data/analysis/scitools/help/gtmktime.txt`
[5] `http://fermi.gsfc.nasa.gov/ssc/data/analysis/scitools/data_preparation.html`

2.2 Point Spread Functions and Location Filtering

`gtpsf`[6] tool requires the livetime map to generate the PSFs. This map is computed by `gtltcube`[7] with the following parameters:

```
gtltcube evfile=timed.fits evtable=EVENTS scfile=[spacecraft] sctable=SC_DATA
       outfile=ltcube.fits
       dcostheta=0.025 binsz=1 phibins=0 tmin=0 tmax=0 zmax=180 zmin=0
```

Having the maps, we can compute the PSFs:

```
gtpsf expcube=ltcube.fits outfile=psf_[IrfName].fits outtable=PSF irfs=[IrfName]
       ra=[RA] dec=[DEC] emin=100 emax=1000000 nenergies=41 thetamax=30 ntheta=300
```

Here `[RA]` and `[DEC]` are the coordinates of the burst, and `[IrfName]` is the Instrument Response Function, which depends on photon's event class (transient, source, clean, or ultraclean) and conversion type (back, or front). The list of IRF names can be obtained by using the `gtirfs`[8] tool. We need to compute PSFs for all of them.

Imagine a stream of photons coming from some source locate at some coordinates θ, ϕ. Ideally, all the coordinates measured for the photons coming from the source should be the same. However, due to measurement errors, they would be spread across some region of the sky. If we find the region such that, say, 95% of photons coming from the source are measured inside of it, we can filter out all the other photons without losing too much statistics, and significantly reducing background. `gtpsf` approximates these regions as circles, and the files generated in the previous step contain the observation probability densities as functions of distance from the source, and photon energies. We, however, need an integral quantity, that is given the radius, we want to know the fraction of photons observed inside the circle of this radius. We can compute this fraction by summing over the probability densities:

$$p(n) = \sum_{i=0}^{n} \frac{\texttt{pdf[i]} + \texttt{pdf[i+1]}}{2} 2\pi \left(\cos\left(\texttt{angles[i]}\right) - \cos\left(\texttt{angles[i+1]}\right)\right)$$

Here `pdf[i]` is the probability density in the point separated from the source by an angle `angles[i]`. And $p(n)$ is the probability to observe a photon closer to the source than `angles[n]`. We find probabilities for intermediate angles by linear interpolation. Finally, we can compute the inverse value $\theta_{\text{spread}}(p)$ (that is a distance as a function of probability) by binary search. Note, that $\theta_{\text{spread}}(p)$ depends on the photon energy, event class, and conversion type. We should use the appropriate function for each photon. The spread angles for intermediate energies are linearly interpolated.

Finally, to finish the filtering, we filter out all the photons, for which their location is separated from the source by more that $\theta_{\text{spread}}(0.95) + \texttt{location.err}$, where `location.err` is the uncertainty in the burst location (see table 1).

Now we have a decent set of photons, which we can use for analysis. However, some of the photons in this set are still originated from background, and not from the source. We cannot filter out these photons, however, we can substitute a linear component of background by estimating it from a long time period before the burst. In order to perform this computation, we'll need an exposure map, which will be discussed in the following section.

2.3 Exposure Maps and Background Estimation

The exposure map can be computed with the `gtexpcube2`[9] tool. We use the following parameter set for it:

[6] `http://fermi.gsfc.nasa.gov/ssc/data/analysis/scitools/help/gtpsf.txt`
[7] `http://fermi.gsfc.nasa.gov/ssc/data/analysis/scitools/help/gtltcube.txt`
[8] `http://fermi.gsfc.nasa.gov/ssc/data/analysis/scitools/help/gtirfs.txt`
[9] `http://fermi.gsfc.nasa.gov/ssc/data/analysis/scitools/help/gtexpcube2.txt`

```
gtexpcube2 infile=ltcube.fits cmap=none outfile=expcube_[IrfName].fits irfs=[IrfName]
       nxpix=360 nypix=180 binsz=1 coordsys=CEL xref=0 yref=0 axisrot=0
       proj=CAR ebinalg=log emin=100 emax=1000000 enumbins=40
       ebinfile=NONE bincalc=EDGE ignorephi=no thmax=180 thmin=0 table=Exposure
```

The generated `expcube` files contain exposures as functions of energy and location on the sky[10]. We use trilinear interpolation to compute exposures for all energies and locations.

Knowing the exposures, we can now use the method introduced in the appendix of [RPT12] to estimate the linear component of background from the data observed before the burst. We compute two background estimates: for low and high energy bands. Because the background of transient class photons may depend on the spacecraft position, we have to filter them as well.

2.4 KS-test

We take care of remaining background by using the following functions with the Kolmogorov-Smirnov test:

$$\Phi_i(t) = \frac{p_i(T_1, t) - b_i \frac{t-T_1}{T_2-T_1}}{p_i(T_1, T_2) - b_i} \tag{1}$$

Here (T_1, T_2) is the time range of observations, $p_i(t_1, t_2)$ is the number of photons observed in the time range t_1 to t_2 in the i's energy band ($i = \text{low}, \text{high}$ are for the low and high energy bands respectfully), and b_i is the estimated number of background photons for the time range T_1 to T_2 in the i's energy band.

The numbers of degrees of freedom (used as an input for the KS-test) are $p_i(T_1, T_2) - b_i$.

While we did not prove it, we assume that the Kolmogorov-Smirnov statistics computed for these functions with provided number of degrees of freedom has a similar distribution to that of the KS-statistics for ordinary CDFs (that is CDFs with no background).

Finally, we compute KS-probabilities for pairs $\Phi_{\text{low}}(t), \Phi_{\text{high}}(\kappa t)$ to obtain the allowed ranges for stretching factors κ. We evaluate stretching factors in the range `STRETCHING_MIN` $= 0.1$ to `STRETCHING_MAX` $= 10.$ with a logarithmic step of `STRETCHING_STEP` $= 1.001$.

As a result of such calculation we can constraint the range of allowed stretching factors to values for which the KS-probabilities are not too small, in other words, given the sigma-significance value, compute the range outside of which stretching factors are elliminated by observations.

You can see the results of such computation in the following section.

2.5 Results

Out of 19 bursts studied, only 4 have at least 10 high energy events remaining after filtering, and thus eligible for the computation of stretching factors. The results of this computation are shown on figures 3, 4, 5, 6 and table 2.

Out of these 4 bursts, two (080916C and 090510) have stretching factors compatible with $\kappa = 1$ within 2σ range.

GRB 090926A has, however, high energy radiation stretched with respect to low energy signal (that is $\kappa > 1$). In contrast to that, GRB 090902B has low energy radiation stretched with respect to high energy signal ($\kappa < 1$).

So we obtained a preliminary (for significance is less than 5σ) result that the stretching factors for observable bursts might be both larger and smaller than 1.

[10] Note, that in the `expcube` FITS files R.A. coordinates are indexed in reverse order and starting from 180, for example, `ra[0]` $= 180$, `ra[1]` $= 179$, and so on.

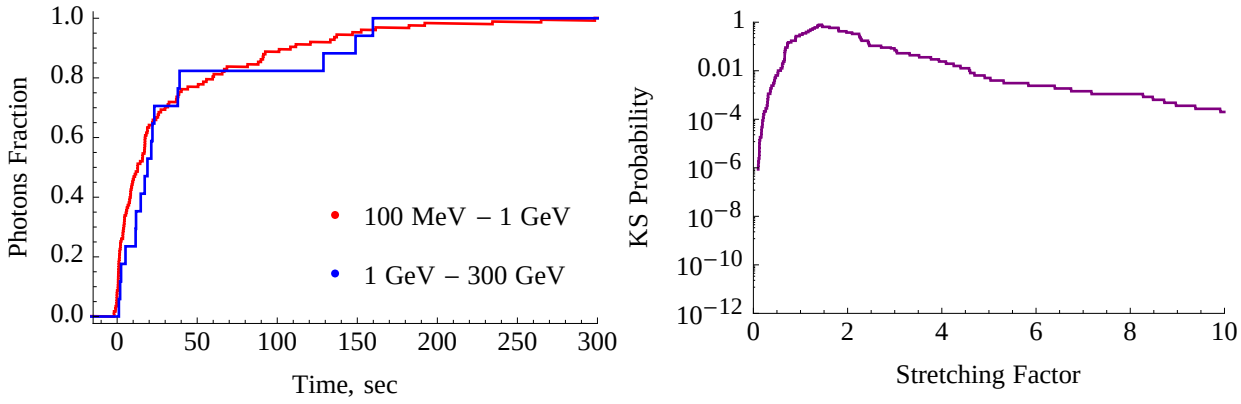

Figure 3: GRB 080916C results. Stretching factor is compatible with $\kappa = 1$ within 2σ.

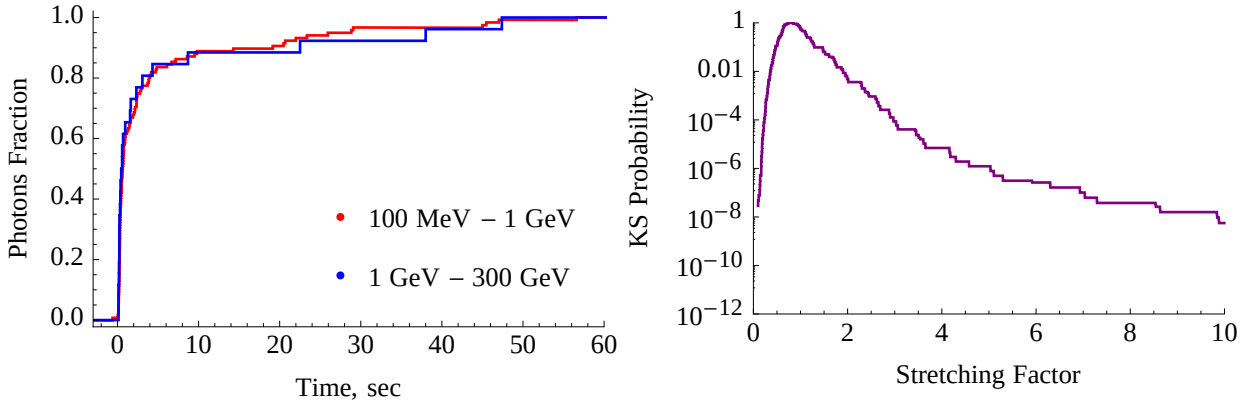

Figure 4: GRB 090510 results. Stretching factor is compatible with $\kappa = 1$ within 1σ.

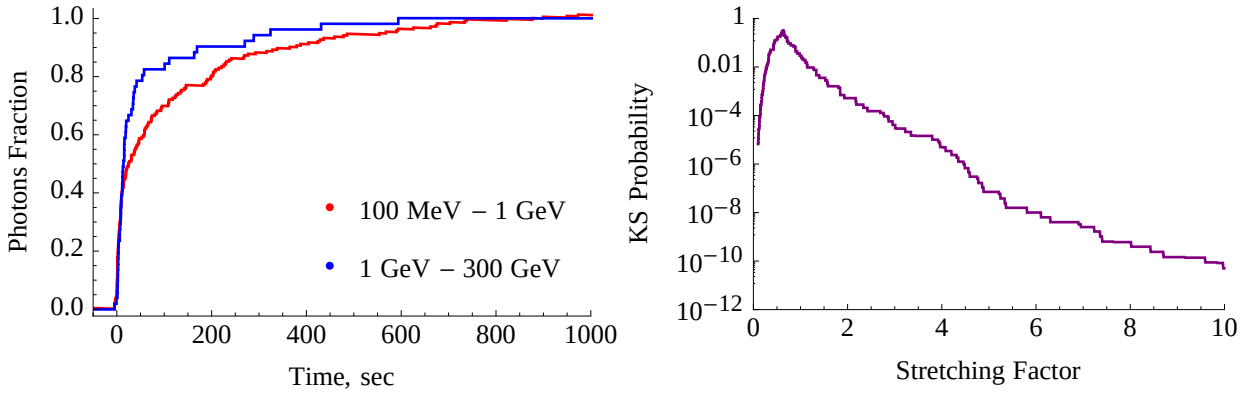

Figure 5: GRB 090902B results. Low energy radiation is stretched ($\kappa < 1$) with significance of 2σ.

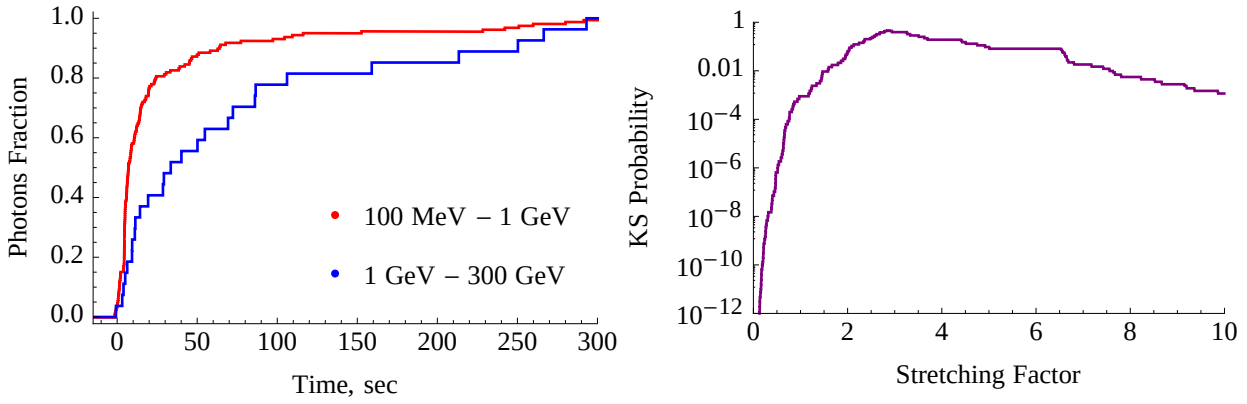

Figure 6: GRB 090926A results. High energy radiation is stretched ($\kappa > 1$) with significance of 3σ.

GRB	1σ	2σ	3σ	4σ	5σ
080825C	1.04 – 2.24	0.67 – 3.32	0.42 – 5.83	0.19 – 14.9	0.087 – 35.7
090501	0.58 – 1.1	0.43 – 1.61	0.32 – 2.29	0.22 – 3.03	0.17 – 5.11
090902B	0.629 – 0.635	0.36 – 0.89	0.23 – 1.57	0.13 – 2.87	0.084 – 4.56
090926A	2.61 – 3.33	1.99 – 6.62	1.34 – 9.15	0.73 – 13.5	0.48 – 19.4

Table 2: Burst observation results. Ranges of allowed stretching factors are shown for studied bursts for multiple levels of significance.

3 Model

3.1 Assumptions

To understand the observed spectral lag, lets explore geometry of the jet. First of all, lets make some assumptions:

1. Time $t = 0$, a spherical shell of plasma is emitted. The center is called the central engine.
2. The shell points propagate with a constant velocity $v \sim 1$, so at the time t the radius of the shall is vt.
3. Each point of the shell is an isotropic radiator in its rest frame.
4. The radiation intensity is a function of the radiator position and the radiation frequency:

$$\eta\left(r,\theta,\omega\right) = \frac{\eta_0}{1+\left(\frac{r}{r_0}\right)^n} \exp\left(-\left(\frac{\theta}{\theta_0}\right)^2 \left(\frac{\omega}{\omega_0}\right)^{-2k}\right) \left(\frac{\omega}{\omega_0}\right)^{\alpha} \tag{2}$$

   η is a number of particles emitted per volume per solid angle per frequency. It is a function of the distance r from the central engine, of the off-axis angle θ, and of the radiation frequency ω.

The burst is fully specified by the following set of parameters:

- v, the velocity of the shell, $\gamma = \frac{1}{\sqrt{1-v^2}} \gg 1$.
- η_0, which defines the luminosity scale.
- r_0, the characteristic jet length; $r_0 \ll \frac{1}{H(0)}$, $H\left(t\right)$ is the Hubble parameter;
- n, which determines the sharpness of the jet end, $n > 3$;

- ω_0, a characteristic radiation frequency;
- θ_0, the opening angle of the jet for radiation with frequency ω_0, $\theta_0 \ll 1$;
- k, which determines how much the opening angle changes with frequency, $k < 0$;
- α, the bare spectral index, $\alpha < -2k - 1$

Now we have all we need to calculate the observed light curves, and then the stretching factors.

3.2 Photon observation time

Lets begin by computing a time at which some particular photon is observed. This time is a function of the radiator location (r, θ, ϕ), as well as the observer location $(d, \chi, 0)$. (Here we choose coordinates so that the rotation angle of the observer is 0.) Lets assume for now that the observer is far enough to resolve the jet geometry, yet close enough so that the expansion of space is negligible. This assumption allows us to ignore the effects of cosmology for this calculation.

The observation time is a sum of two terms: the time interval from $t = 0$ to the photon emission (the plasma time), and the time interval between the emission and the observation (the photon time):

$$t\left(r, \theta, \phi, d, \chi\right) = t_{\text{plasma}}\left(r\right) + t_{\text{photon}}\left(r, \theta, \phi, d, \chi\right)$$

t_{plasma} is easy to compute since plasma moves with uniform velocity:

$$t_{\text{plasma}}\left(r\right) = \frac{r}{v}$$

t_{photon} is a distance between the radiator and the observer:

$$\begin{aligned}
t_{\text{photon}}\left(r, \theta, \phi, d, \chi\right) &= \sqrt{\left(d\cos\chi - r\cos\theta\right)^2 + \left(d\sin\chi - r\sin\theta\cos\phi\right)^2 + \left(r\sin\theta\sin\phi\right)^2} \\
&= d\sqrt{\left(\cos\chi - \frac{r}{d}\cos\theta\right)^2 + \left(\sin\chi - \frac{r}{d}\sin\theta\cos\phi\right)^2 + \left(\frac{r}{d}\sin\theta\sin\phi\right)^2} \\
&\sim d\sqrt{\cos^2\chi - 2\frac{r}{d}\cos\theta\cos\chi + \sin^2\chi - 2\frac{r}{d}\sin\theta\cos\phi\sin\chi} \\
&\sim d\left(1 - \frac{r}{d}\left(\cos\theta\cos\chi + \sin\theta\cos\phi\sin\chi\right)\right) \\
&= d - r\left(\cos\theta\cos\chi + \sin\theta\cos\phi\sin\chi\right)
\end{aligned}$$

Combining these expressions together, we get:

$$t\left(r, \theta, \phi, d, \chi\right) = d + r\left(\frac{1}{v} - \cos\theta\cos\chi - \sin\theta\cos\phi\sin\chi\right)$$

Since no photon can reach the observer faster than the speed of light, and the photons emitted at $t = 0$ reach the observer at $t = d$, this time $t = d$ is the start of the observer's light curve. So we can define a more convenient time origin:

$$\tau\left(r, \theta, \phi, \chi\right) = t\left(r, \theta, \phi, d, \chi\right) - d = r\left(\frac{1}{v} - \cos\theta\cos\chi - \sin\theta\cos\phi\sin\chi\right)$$

Finally, we can use the spherical law of cosines to write this in terms of the great-circle distance $\sigma\left(\theta, \phi, \chi\right)$ between the points (θ, ϕ) and $(\chi, 0)$:

$$\tau\left(r, \theta, \phi, \chi\right) = r\left(\frac{1}{v} - \cos\sigma\left(\theta, \phi, \chi\right)\right) \tag{3}$$

Note that τ doesn't depend on d anymore. But this is only true if the scale factor did not change since emission to observation. For a distant observer we should account for the change in the scale factor, which will stretch the distances between photons:

$$\tau\left(r,\theta,\phi,z,\chi\right)=r\left(\frac{1}{v}-\cos\sigma\left(\theta,\phi,\chi\right)\right)\left(1+z\right) \tag{4}$$

Here z is the redshift of the burst from the point of view of the observer.

3.3 Cosmology

Before calculating light curves and stretching factors, we will need some equations from cosmology.

First of all, the metric of the expanding Universe:

$$\mathrm{d}s^2=-\,\mathrm{d}t^2+a^2\left(t\right)\mathrm{d}r^2+a^2\left(t\right)r^2\,\mathrm{d}\Omega_2 \tag{5}$$

We define $a\left(t_{\mathrm{obs}}\right)=1$, where t_{obs} is the observation time.

We need to understand how the scale factor changes with time. For that we assume that the energy content of the Universe consists of matter Ω_m and vacuum energy Ω_Λ only, so that the Friedmann equation takes the following form:

$$\begin{aligned}\left(\frac{\dot{a}\left(t\right)}{a\left(t\right)}\right)^2&=\Omega_m H_{\mathrm{obs}}^2\frac{1}{a^3\left(t\right)}+H_{\mathrm{obs}}^2\Omega_\Lambda\\ \dot{a}\left(t\right)&=a\left(t\right)H_{\mathrm{obs}}\sqrt{\Omega_m\frac{1}{a^3\left(t\right)}+\Omega_\Lambda}\\ \mathrm{d}t&=\frac{\mathrm{d}a}{a\left(t\right)H_{\mathrm{obs}}\sqrt{\Omega_m\frac{1}{a^3(t)}+\Omega_\Lambda}}\end{aligned}$$

Here $H_{\mathrm{obs}}=H\left(t_{\mathrm{obs}}\right)=\dot{a}\left(t_{\mathrm{obs}}\right)$ is the Hubble parameter at the observation time.

We also need to know the areas of two spheres: the photon sphere, a sphere over which photons emitted in a particular burst are spread; and the bursts sphere, a sphere over which bursts at a particular redshift are distributed.

Lets begin with the photon sphere. This sphere has the origin at $r=0$ and $t=0$, at the central engine of a particular burst. Taking $\mathrm{d}s=0$ and $\mathrm{d}\Omega_2=0$ in the equation for metric, we get:

$$\mathrm{d}r=\frac{\mathrm{d}t}{a\left(t\right)}$$

And now we integrate over time to find the observer's position:

$$\begin{aligned}r\left(t_{\mathrm{obs}}\right)&=\int_0^{t_{\mathrm{obs}}}\frac{\mathrm{d}t}{a\left(t\right)}\\ &=\int_{a(0)}^{1}\frac{\mathrm{d}a}{a^2\left(t\right)H_{\mathrm{obs}}\sqrt{\Omega_m\frac{1}{a^3(t)}+\Omega_\Lambda}}\\ &=\frac{{}_2F_1\left(\frac{1}{3},\frac{1}{2};\frac{4}{3};-\frac{\Omega_m}{a^3(0)\Omega_\Lambda}\right)-a\left(0\right){}_2F_1\left(\frac{1}{3},\frac{1}{2};\frac{4}{3};-\frac{\Omega_m}{\Omega_\Lambda}\right)}{a\left(0\right)H_{\mathrm{obs}}\sqrt{\Omega_\Lambda}}\end{aligned}$$

Here ${}_2F_1\left(a,b;c;z\right)=\frac{\Gamma(c)}{\Gamma(b)\Gamma(c-b)}\int_0^1\frac{t^{b-1}(1-t)^{c-b-1}}{(1-tz)^a}\,\mathrm{d}t$ is a hypergeometric function. Here $a\left(0\right)=\frac{1}{1+z}$, so, finally,

$$r\left(z\right)=\frac{\left(1+z\right){}_2F_1\left(\frac{1}{3},\frac{1}{2};\frac{4}{3};-\frac{\Omega_m}{\Omega_\Lambda}\left(1+z\right)^3\right)-{}_2F_1\left(\frac{1}{3},\frac{1}{2};\frac{4}{3};-\frac{\Omega_m}{\Omega_\Lambda}\right)}{H_{\mathrm{obs}}\sqrt{\Omega_\Lambda}} \tag{6}$$

The area of the photon sphere is then:

$$A_{\mathrm{ph}}(z) = 4\pi a^2(t_{\mathrm{obs}})\, r^2(z) = 4\pi r^2(z) \tag{7}$$

The second sphere is the bursts sphere. It has its origin at the observer's position. We define a new primed set of coordinates, so that $r' = 0$ and $t' = 0$ at the observation event. We can relate the primed coordinates of the burst to the observer's unprimed coordinates:

$$\begin{aligned} t'_{\mathrm{burst}} &= -t_{\mathrm{obs}} \\ r'\left(t'_{\mathrm{burst}}\right) = r'\left(-t_{\mathrm{obs}}\right) &= \int_{-t_{\mathrm{obs}}}^{0} \frac{\mathrm{d}t'}{a'(t')} = \int_{0}^{t_{\mathrm{obs}}} \frac{\mathrm{d}t}{a(t)} = r(t_{\mathrm{obs}}) \end{aligned}$$

We see that the radius of the bursts sphere is the same as the radius of the photon sphere. Finally, the area is:

$$A_{\mathrm{b}}(z) = 4\pi a'^2(-t_{\mathrm{obs}})\, r^2(z) = 4\pi a^2(0)\, r^2(z) = \frac{4\pi r^2(z)}{(1+z)^2} \tag{8}$$

We will need to know one more thing about the bursts sphere – the volume of the infinitesimal shell surrounding it. For that we can again use the metric:

$$\begin{aligned} \mathrm{d}V(z) &= -A_{\mathrm{b}}(z)\, a(0)\, \mathrm{d}r \\ &= -A_{\mathrm{b}}(z)\, a(0)\, \frac{\mathrm{d}a}{a^2(0)\, H_{\mathrm{obs}} \sqrt{\Omega_m \frac{1}{a^3(t)} + \Omega_\Lambda}} \\ &= A_{\mathrm{b}}(z)\, \frac{\frac{1}{(1+z)^2}\, \mathrm{d}z\, (1+z)}{H_{\mathrm{obs}} \sqrt{\Omega_m \frac{1}{a^3(t)} + \Omega_\Lambda}} \\ &= A_{\mathrm{b}}(z)\, \frac{1}{(1+z)}\, \frac{\mathrm{d}z}{H_{\mathrm{obs}} \sqrt{\Omega_m (1+z)^3 + \Omega_\Lambda}} \\ &= \frac{4\pi r^2(z)}{(1+z)^3}\, \frac{\mathrm{d}z}{H_{\mathrm{obs}} \sqrt{\Omega_m (1+z)^3 + \Omega_\Lambda}} \end{aligned} \tag{9}$$

3.4 Light curve

We now know enough to compute the observable quantity - the number of observed photons p. For that we need to integrate the radiation intensity η over four things. Two burst-related things: radiator positions and frequencies at emission. Two observer-related things: observation time and frequencies at observation. We relate the first two and the second two with the delta functions:

$$\begin{aligned} p(z, \chi; \tau_1, \tau_2; \omega_1, \omega_2) = \frac{A_{\mathrm{det}}}{A_{\mathrm{ph}}(z)} \int_0^\infty \mathrm{d}r \int_0^\pi r\, \mathrm{d}\theta \int_0^{2\pi} r \sin\theta\, \mathrm{d}\phi \int_0^\infty \mathrm{d}\omega' \int_{\tau_1}^{\tau_2} \mathrm{d}\tau \int_{\omega_1}^{\omega_2} \mathrm{d}\omega\, \eta\left(r, \theta, \omega'\right) \\ \times \underbrace{\frac{1}{\gamma^2\left(1 - v\cos\sigma(\theta, \phi, \chi)\right)^2}}_{\text{aberration}} \underbrace{\frac{1}{\gamma\left(1 - v\cos\sigma(\theta, \phi, \chi)\right)}}_{\text{time dilation}} \\ \times \delta\left(\underbrace{\frac{\omega'}{\gamma\left(1 - v\cos\sigma(\theta, \phi, \chi)\right)}}_{\text{relativistic shift}} \underbrace{(1+z)}_{\text{cosmological shift}} - \omega \right) \end{aligned}$$

$$\times \delta\left(\tau - r\left(\frac{1}{v} - \cos\sigma\left(\theta,\phi,\chi\right)\right)\left(1+z\right)\right) \tag{10}$$

Here $A_{\rm det}$ is the effective area of the detector. We have taken account for the four relativistic effects, which affect intensities and frequencies of the radiators: relativistic aberration; time dilation of the radiators relative to the observer; relativistic blue/redshift; and cosmological redshift.

We can use the delta functions to do the integrals over ω' and r. For that lets transform the first one:

$$\begin{aligned}\delta\left(\frac{\omega'}{\gamma\left(1-v\cos\sigma\right)\left(1+z\right)} - \omega\right) &= \delta\left(\frac{1}{\gamma\left(1-v\cos\sigma\right)\left(1+z\right)}\left(\omega' - \gamma\left(1-v\cos\sigma\right)\left(1+z\right)\omega\right)\right)\\ &= \gamma\left(1-v\cos\sigma\right)\left(1+z\right)\delta\left(\omega' - \gamma\left(1-v\cos\sigma\right)\left(1+z\right)\omega\right)\end{aligned}$$

And the second one:

$$\begin{aligned}\delta\left(\tau - r\left(\frac{1}{v} - \cos\sigma\right)\left(1+z\right)\right) &= \delta\left(\left(\frac{1}{v} - \cos\sigma\right)\left(1+z\right)\left(r - \frac{\tau}{\left(\frac{1}{v} - \cos\sigma\right)\left(1+z\right)}\right)\right)\\ &= \frac{1}{\left(\frac{1}{v} - \cos\sigma\right)\left(1+z\right)}\delta\left(r - \frac{\tau}{\left(\frac{1}{v} - \cos\sigma\right)\left(1+z\right)}\right)\end{aligned}$$

After the transformations the expression for p takes the following form:

$$\begin{aligned}p\left(z,\chi;\tau_1,\tau_2;\omega_1,\omega_2\right) = \frac{A_{\rm det}}{A_{\rm ph}\left(z\right)}&\int_0^{\pi}{\rm d}\theta\int_0^{2\pi}{\rm d}\phi\int_{\tau_1}^{\tau_2}{\rm d}\tau\int_{\omega_1}^{\omega_2}{\rm d}\omega\\ &\times\eta\left(\frac{\tau}{\left(\frac{1}{v}-\cos\sigma\left(\theta,\phi,\chi\right)\right)\left(1+z\right)},\theta,\gamma\left(1-v\cos\sigma\left(\theta,\phi,\chi\right)\right)\left(1+z\right)\omega\right)\\ &\times\frac{\tau^2\sin\theta}{\left(\frac{1}{v}-\cos\sigma\left(\theta,\phi,\chi\right)\right)^3\left(1+z\right)^2\gamma^2\left(1-v\cos\sigma\left(\theta,\phi,\chi\right)\right)^2}\\ = \frac{A_{\rm det}}{A_{\rm ph}\left(z\right)}\frac{1}{v^2\gamma^2\left(1+z\right)^2}&\int_{\tau_1}^{\tau_2}{\rm d}\tau\,\tau^2\int_0^{\frac{\pi}{2}}{\rm d}\theta\int_0^{2\pi}{\rm d}\phi\int_{\omega_1}^{\omega_2}{\rm d}\omega\frac{\sin\theta}{\left(\frac{1}{v}-\cos\sigma\left(\theta,\phi,\chi\right)\right)^5}\\ &\times\eta\left(\frac{\tau}{\left(\frac{1}{v}-\cos\sigma\left(\theta,\phi,\chi\right)\right)\left(1+z\right)},\theta,\gamma\left(1-v\cos\sigma\left(\theta,\phi,\chi\right)\right)\left(1+z\right)\omega\right)\end{aligned} \tag{11}$$

Furthermore, we can do the integrals over ω and τ, if we write η explicitly:

$$\begin{aligned}p\left(z,\chi;\tau_1,\tau_2;\omega_1,\omega_2\right) = \frac{A_{\rm det}}{A_{\rm ph}\left(z\right)}\frac{1}{v^2\gamma^2\left(1+z\right)^2}&\int_0^{\pi}{\rm d}\theta\int_0^{2\pi}{\rm d}\phi\int_{\omega_1}^{\omega_2}{\rm d}\omega\int_{\tau_1}^{\tau_2}{\rm d}\tau\,\tau^2\frac{\sin\theta}{\left(\frac{1}{v}-\cos\sigma\left(\theta,\phi,\chi\right)\right)^5}\\ &\times\frac{\eta_0}{1+\left(\frac{\tau}{r_0\left(\frac{1}{v}-\cos\sigma\left(\theta,\phi,\chi\right)\right)\left(1+z\right)}\right)^n}\\ &\times\exp\left(-\left(\frac{\theta}{\theta_0}\right)^2\left(\frac{\omega\gamma\left(1-v\cos\sigma\left(\theta,\phi,\chi\right)\right)\left(1+z\right)}{\omega_0}\right)^{-2k}\right)\\ &\times\left(\frac{\omega\gamma\left(1-v\cos\sigma\left(\theta,\phi,\chi\right)\right)\left(1+z\right)}{\omega_0}\right)^{\alpha}\\ = \frac{A_{\rm det}}{A_{\rm ph}\left(z\right)}\frac{\eta_0}{\left(v\gamma\left(1+z\right)\right)^{2-\alpha}}&\int_0^{\pi}{\rm d}\theta\int_0^{2\pi}{\rm d}\phi\frac{\sin\theta}{\left(\frac{1}{v}-\cos\sigma\left(\theta,\phi,\chi\right)\right)^{5-\alpha}}\end{aligned}$$

$$\times \int_{\omega_1}^{\omega_2} \mathrm{d}\omega \exp\left(-\left(\frac{\theta}{\theta_0}\right)^2 \left(\frac{\omega\gamma\left(1 - v\cos\sigma\left(\theta,\phi,\chi\right)\right)(1+z)}{\omega_0}\right)^{-2k}\right)\left(\frac{\omega}{\omega_0}\right)^{\alpha}$$
$$\times \int_{\tau_1}^{\tau_2} \mathrm{d}\tau\, \tau^2 \frac{1}{1+\left(\frac{\tau}{r_0\left(\frac{1}{v}-\cos\sigma(\theta,\phi,\chi)\right)(1+z)}\right)^n}$$
$$= \frac{A_{\mathrm{det}}}{A_{\mathrm{ph}}\left(z\right)} \frac{\eta_0}{\left(v\gamma\left(1+z\right)\right)^{2-\alpha}} \int_0^{\pi} \mathrm{d}\theta \int_0^{2\pi} \mathrm{d}\phi \frac{\sin\theta}{\left(\frac{1}{v} - \cos\sigma\left(\theta,\phi,\chi\right)\right)^{5-\alpha}}$$
$$\times \left(I\left(z,\chi,\omega_2;\theta,\phi\right) - I\left(z,\chi,\omega_1;\theta,\phi\right)\right)\left(J\left(z,\chi,\tau_2;\theta,\phi\right) - J\left(z,\chi,\tau_1;\theta,\phi\right)\right) \quad (12)$$

Here I and J are the indefinite integrals over ω and τ:

$$I\left(z,\chi,\omega;\theta,\phi\right) = \frac{\omega\left(\frac{\omega}{\omega_0}\right)^{\alpha} E_{\frac{\alpha+1}{2k}+1}\left(\left(\frac{\theta}{\theta_0}\right)^2\left(\frac{\omega}{\omega_0}\right)^{-2k}\left(\gamma\left(1 - v\cos\sigma\left(\theta,\phi,\chi\right)\right)(1+z)\right)^{-2k}\right)}{2k} \quad (13)$$

$$J\left(z,\chi,\tau;\theta,\phi\right) = \frac{\tau^3}{3}\,{}_2F_1\left(1,\frac{3}{n};\frac{n+3}{n};-\left(\frac{\tau}{r_0\left(\frac{1}{v}-\cos\sigma\left(\theta,\phi,\chi\right)\right)(1+z)}\right)^n\right) \quad (14)$$

where E_n function $E_n\left(x\right) = \int_1^{\infty} \frac{e^{-xt}\,\mathrm{d}t}{t^n}$.

The remaining integrals over θ and χ are hard to do symbolically, so we compute them numerically. To optimize this computation we can use the assumption of small θ and χ, so that:

$$\sin\theta \sim \theta$$
$$\cos\sigma\left(\theta,\phi,\chi\right) = \cos\theta\cos\chi + \sin\theta\sin\chi\cos\phi \sim 1 - \frac{\theta^2}{2} - \frac{\chi^2}{2} + \theta\chi\cos\phi$$

Using that, and the observation that this integral is an even function of θ, we arrive to the optimized expressions for p, I and J:

$$p\left(z,\chi;\tau_1,\tau_2;\omega_1,\omega_2\right) = \frac{A_{\mathrm{det}}}{A_{\mathrm{ph}}\left(z\right)} \frac{2\eta_0}{\left(v\gamma\left(1+z\right)\right)^{2-\alpha}} \int_0^{\infty} \mathrm{d}\theta \int_0^{\pi} \mathrm{d}\phi \frac{\theta}{\left(\frac{1}{v} - 1 + \frac{\theta^2}{2} + \frac{\chi^2}{2} - \theta\chi\cos\phi\right)^{5-\alpha}}$$
$$\times \left(I\left(z,\chi,\omega_2;\theta,\phi\right) - I\left(z,\chi,\omega_1;\theta,\phi\right)\right)\left(J\left(z,\chi,\tau_2;\theta,\phi\right) - J\left(z,\chi,\tau_1;\theta,\phi\right)\right) \quad (15)$$

$$I\left(z,\chi,\omega;\theta,\phi\right) = \frac{\omega\left(\frac{\omega}{\omega_0}\right)^{\alpha} E_{\frac{\alpha+1}{2k}+1}\left(\left(\frac{\theta}{\theta_0}\right)^2\left(\frac{\omega}{\omega_0}\right)^{-2k}\left(v\gamma\left(1+z\right)\left(\frac{1}{v} - 1 + \frac{\theta^2}{2} + \frac{\chi^2}{2} - \theta\chi\cos\phi\right)\right)^{-2k}\right)}{2k} \quad (16)$$

$$J\left(z,\chi,\tau;\theta,\phi\right) = \frac{\tau^3}{3}\,{}_2F_1\left(1,\frac{3}{n};\frac{n+3}{n};-\left(\frac{\tau}{r_0\left(\frac{1}{v} - 1 + \frac{\theta^2}{2} + \frac{\chi^2}{2} - \theta\chi\cos\phi\right)(1+z)}\right)^n\right) \quad (17)$$

Finally, we will need to compute limits of p for $\omega_2 \to \infty$ and $\tau_2 \to \infty$. It requires us to know the limit of I for $\omega \to \infty$ (we assumed that $k < 0$):

$$I\left(z,\chi,\infty;\theta,\phi\right) = \lim_{\omega\to\infty} I\left(z,\chi,\omega;\theta,\phi\right) = 0 \quad (18)$$

and the limit of J for $\tau \to \infty$ ($n > 3$ by assumption):

$$J\left(z,\chi,\infty;\theta,\phi\right) = \lim_{\tau\to\infty} J\left(z,\chi,\tau;\theta,\phi\right) = \left(r_0\left(\frac{1}{v} - 1 + \frac{\theta^2}{2} + \frac{\chi^2}{2} - \theta\chi\cos\phi\right)(1+z)\right)^3 \frac{\pi}{n\sin\frac{3\pi}{n}} \quad (19)$$

Now, when we know p, we can compute many different things with it. Examples include:

- the total number of particles observed in a given energy range, $p_\infty(z,\chi;\omega_1,\omega_2) = p(z,\chi;0,\infty;\omega_1,\omega_2)$;
- the fraction of photons observed during a given time interval, $\Phi(z,\chi;\tau_1,\tau_2;\omega_1,\omega_2) = \frac{p(z,\chi;\tau_1,\tau_2;\omega_1,\omega_2)}{p_\infty(z,\chi;\omega_1,\omega_2)}$;
- the duration of the burst $T_f(z,\chi;\omega_1,\omega_2)$, that is the time by which the fraction f of photons is observed. We can compute it by solving the following equation for T_f: $p\left(z,\chi;0,T_f;\omega_1,\omega_2\right) = f p_\infty(z,\chi;\omega_1,\omega_2)$;
- the stretching factor, which we will discuss in the next section.

3.5 Stretching factor

The stretching factor for a continuous light curve is defined exactly like the stretching factor for a discrete one. It is the value of κ which makes the KS-distance minimal:

$$\kappa(z,\chi;\omega_1,\omega_2,\omega_3) = \operatorname*{argmin}_\kappa \max_\tau \left|\Phi(z,\chi;0,\tau;\omega_1,\omega_2) - \Phi(z,\chi;0,\kappa\tau;\omega_2,\omega_3)\right| \tag{20}$$

The maximum of an absolute value cannot be differentiated, so the computation of κ by the given definition is complicated. Lets instead rewrite this expression in terms of a positive and a negative KS-distances:

$$\begin{aligned}
D_+(z,\chi;\kappa;\omega_1,\omega_2,\omega_3) &= \max_\tau \left(\Phi(z,\chi;0,\tau;\omega_1,\omega_2) - \Phi(z,\chi;0,\kappa\tau;\omega_2,\omega_3)\right)\\
D_-(z,\chi;\kappa;\omega_1,\omega_2,\omega_3) &= \min_\tau \left(\Phi(z,\chi;0,\tau;\omega_1,\omega_2) - \Phi(z,\chi;0,\kappa\tau;\omega_2,\omega_3)\right)\\
\kappa(z,\chi;\omega_1,\omega_2,\omega_3) &= \operatorname*{argmin}_\kappa \max\left(D_+(z,\chi;\kappa;\omega_1,\omega_2,\omega_3), -D_-(z,\chi;\kappa;\omega_1,\omega_2,\omega_3)\right)
\end{aligned}$$

Take note that Φ monotonously increases with τ. It implies that D_+ and D_- monotonously decrease with κ, so as $D_+ + D_-$. So there is a single value of κ, for which

$$D_+(z,\chi;\kappa;\omega_1,\omega_2,\omega_3) = -D_-(z,\chi;\kappa;\omega_1,\omega_2,\omega_3) \tag{21}$$

And this value of κ also makes the $\max(D_+,-D_-)$ minimal, since D_+ monotonously decrease, and $-D_-$ monotonously increase with κ.

So we have now a simpler way to compute κ by solving an equation instead of computing the minimum. And Φ can be differentiated, which makes it easier to compute maximums and minimums of their differences.

Being able to compute the stretching factor, we could now compare our model predictions with observations given the position of an observer. We don't know the observer's off-axis angle χ, however, so we cannot check the stretching factor prediction directly. Instead, we will focus on a series of tests, which will ensure that our model doesn't contradict existing observations. These tests will be discussed in the following sections.

3.6 Total energy

The first test is to compute the total energy radiated from the burst, and to ensure that it doesn't exceed the mass of the star from which the burst originated.

To compute the total energy, we need to multiply the radiation intensity by frequency, and integrate it over frequencies ω, volume (r,θ,ϕ), and observer positions (σ,ξ). We assumed $\theta \ll 1$, and have taken into account the same relativistic effects as we did in the observed particle count computation:

$$E = \int_0^\infty \mathrm{d}\omega \int_0^\infty \mathrm{d}r \int_0^\infty r\,\mathrm{d}\theta \int_0^{2\pi} r\,\theta\,\mathrm{d}\phi \int_0^\infty \mathrm{d}\sigma \int_0^{2\pi} \sin\sigma\,\mathrm{d}\xi$$

$$\times \eta\left(r,\theta,\omega\right)\underbrace{\frac{1}{\gamma\left(1-v\cos\sigma\right)}}_{\text{time dilation}}\underbrace{\frac{1}{\gamma^2\left(1-v\cos\sigma\right)^2}}_{\text{aberration}}\underbrace{\frac{\omega}{\gamma\left(1-v\cos\sigma\right)}}_{\text{relativistic shift}} \tag{22}$$

$$= \frac{4\pi^2}{\gamma^4}\int_0^\infty \mathrm{d}\omega\,\omega\int_0^\infty \mathrm{d}r\,r^2\int_0^\infty \mathrm{d}\theta\,\theta\,\eta\left(r,\theta,\omega\right)\int_0^\infty \mathrm{d}\sigma\frac{\sin\sigma}{\left(1-v\cos\sigma\right)^4}$$

An integral over σ is computable analytically:

$$\int_0^\infty \mathrm{d}\sigma\frac{\sin\sigma}{\left(1-v\cos\sigma\right)^4} = \frac{2\left(3+v^2\right)}{3\left(1-v^2\right)^3} = \frac{2}{3}\gamma^6\left(4-\frac{1}{\gamma^2}\right)$$

Substituting this result into the expression for E we get:

$$E = \frac{32\pi^2}{3}\left(\gamma^2-\frac{1}{4}\right)\int_0^\infty \mathrm{d}\omega\,\omega\int_0^\infty \mathrm{d}r\,r^2\int_0^\infty \mathrm{d}\theta\,\theta\,\eta\left(r,\theta,\omega\right) \tag{23}$$

Now we can use the expression for η to do the remaining integrals:

$$E = \frac{32\pi^2\eta_0}{3}\left(\gamma^2-\frac{1}{4}\right)\int_0^\infty \mathrm{d}\omega\,\omega\left(\frac{\omega}{\omega_0}\right)^\alpha\int_0^\infty \mathrm{d}r\,\frac{r^2}{1+\left(\frac{r}{r_0}\right)^n}\int_0^\infty \mathrm{d}\theta\,\theta\,\exp\left(-\left(\frac{\theta}{\theta_0}\right)^2\left(\frac{\omega}{\omega_0}\right)^{-2k}\right)$$

The integrals over r and θ can be done symbolically:

$$\int_0^\infty \mathrm{d}r\,\frac{r^2}{1+\left(\frac{r}{r_0}\right)^n} = \frac{\pi}{n\sin\left(\frac{3\pi}{n}\right)}r_0^3$$

$$\int_0^\infty \mathrm{d}\theta\,\theta\,\exp\left(-\left(\frac{\theta}{\theta_0}\right)^2\left(\frac{\omega}{\omega_0}\right)^{-2k}\right) = \frac{1}{2}\theta_0^2\left(\frac{\omega}{\omega_0}\right)^{2k}$$

Now we only have one integral left:

$$E = \frac{16\pi^3}{3n\sin\left(\frac{3\pi}{n}\right)}\left(\gamma^2-\frac{1}{4}\right)\eta_0\,r_0^3\,\theta_0^2\int_0^\infty \mathrm{d}\omega\,\omega\left(\frac{\omega}{\omega_0}\right)^{2k+\alpha} \tag{24}$$

Note, however, that since $\alpha < -2k-1$ this integral diverges for $\omega \to 0$. But our model is not expected to describe low-energy radiation of the burst, so we should not integrate over low-frequency radiators. Nevertheless, we should ensure that the total energy of the high-energy radiation is not too large. To compute this energy we will only integrate over those radiators which emission we can observe, that is over the radiators with frequencies greater than $\frac{\omega_1}{\gamma}$, where ω_1 is the smallest observable photon frequency. Now we can compute the last integral and get the final expression for E:

$$\begin{aligned}
E\left(\omega_1\right) &= \frac{16\pi^3}{3n\sin\left(\frac{3\pi}{n}\right)}\left(\gamma^2-\frac{1}{4}\right)\eta_0\,r_0^3\,\theta_0^2\int_{\frac{\omega_1}{\gamma}}^\infty \mathrm{d}\omega\,\omega\left(\frac{\omega}{\omega_0}\right)^{2k+\alpha} \\
&= \frac{16\pi^3}{3n\sin\left(\frac{3\pi}{n}\right)}\left(\gamma^2-\frac{1}{4}\right)\eta_0\,r_0^3\,\theta_0^2\frac{\omega_1^2\left(\frac{\omega_1}{\gamma\omega_0}\right)^{2k+\alpha}}{\gamma^2(-2k-\alpha-2)} \\
&= \frac{16\pi^3}{3n\left(-2k-\alpha-2\right)\sin\left(\frac{3\pi}{n}\right)}\gamma^{-2k-\alpha}\left(1-\frac{1}{4\gamma^2}\right)\eta_0\,r_0^3\,\theta_0^2\frac{\omega_0^{-2k-\alpha}}{\omega_1^{-2k-\alpha-2}}
\end{aligned} \tag{25}$$

This energy should not be larger than a typical mass M_s of a massive star. So, finally, we arrive at the first constraint for the burst parameters:

$$\frac{16\pi^3}{3n\left(-2k-\alpha-2\right)\sin\left(\frac{3\pi}{n}\right)}\gamma^{-2k-\alpha}\left(1-\frac{1}{4\gamma^2}\right)\eta_0\,r_0^3\,\theta_0^2\frac{\omega_0^{-2k-\alpha}}{\omega_1^{-2k-\alpha-2}} < M_s \tag{26}$$

3.7 Distribution of stretching factors

The second test is to calculate the distribution of the stretching factors of the observable bursts, and to compare it with observations.

The computation of the exact and precise distribution is technically hard (because stretching factors neither change monotonously with redshift, nor with off-axis angle), and computationally intensive. So we will not compute the precise distribution.

Instead, we will use the Monte-Carlo method to produce a large representative sample of stretching factors. Then, we will calculate an empirical CDF of this sample, which can be compared with observations using the KS-test. Since we can compute much larger sample than that of observations, we will not lose much precision due to this simplification.

We still have one ingredient missing though – the evolution of the bursts density. We assume that the density is roughly proportional to the stars density, and the stars density is roughly proportional to the matter density, which changes with z as $(1+z)^3$. It is clear, however, that since no stars existed at very small redshifts, the burst density should decline there, so we add an exponential cutoff to it:

$$\rho = \rho_0 (1+z)^3 \exp\left(-\frac{z}{z_c}\right) \tag{27}$$

Here ρ_0 is a normalization factor, and z_c is a redshift scale, after which the density is cut off.

Now when we have all the ingredients, we can compute the sample with the following steps:

1. First of all we need to define the range from which to select redshifts and off-axis angles. We should include all observable jet positions in this range. However, to avoid dropping too many points corresponding to invisible bursts, we should keep the range as small as possible. We also want to make the region rectangular to be able to select redshifts and angles separately.

   Lets start by selecting a range for redshifts. Ideally, we want this range to start with $z = 0$. Then, however, there will be visible jets for all possible off-axis angles, which will make our angles range too large. Note also, that since the bursts count increases with redshift as z^3, the probability to observe a low-redshift burst is very small. So instead of selecting the smallest redshift to be 0, we select it to be a small number $z_{\min}$.

   $z_{\max}$ is defined by the farthest jet, which can be observed. Since the burst observability $p_\infty(z, \chi, \omega_2, \omega_3)$ decreases with both redshift and χ, we can find the maximum redshift by solving the following equation:

   $$p_\infty(z_{\max}, 0, \omega_2, \omega_3) = p_{\min} \tag{28}$$

   where $p_{\min}$ is the minimum number of particles required to claim an observation.

2. The range for off-axis angles is easier to compute since nothing prohibits us from selecting the smallest angle to be 0.

   The observability declines with z and χ, so the observable burst with the largest χ should be located at the redshift $z_{\min}$. We can find this angle by solving the similar equation, as we did for the redshifts:

   $$p_\infty(z_{\min}, \chi_{\max}, \omega_2, \omega_3) = p_{\min} \tag{29}$$

3. Now we are in a position to select a particular properly distributed random redshift. The CDF of the distribution of redshifts is a ratio of redshift counts in different space volumes:

   $$\Phi_z(z) = \frac{\int_{z_{\min}}^{z} \rho(z')\, \mathrm{d}V(z')}{\int_{z_{\max}}^{z_{\max}} \rho(z')\, \mathrm{d}V(z')} \tag{30}$$

   To generate a redshift, we should uniformly select a value of Φ_z, and solve the corresponding equation for z:

   $$\Phi_z(z) = x \tag{31}$$

   where x is a random variable uniformly distributed in the range 0 to 1.

4. An off-axis angle can be selected in a similar way. The CDF of the angles distribution is a ratio of spherical areas:

$$\Phi_\chi(\chi) = \frac{\int_0^\chi \sin\chi' \,\mathrm{d}\chi'}{\int_0^{\chi_{\max}} \sin\chi' \,\mathrm{d}\chi'} \approx \frac{\int_0^\chi \chi' \,\mathrm{d}\chi'}{\int_0^{\chi_{\max}} \chi' \,\mathrm{d}\chi'} = \left(\frac{\chi}{\chi_{\max}}\right)^2 \tag{32}$$

As with redshifts, we get a properly distributed χ by solving the equation:

$$\Phi_\chi(\chi) = \left(\frac{\chi}{\chi_{\max}}\right)^2 = y \tag{33}$$

$$\chi = \chi_{\max}\sqrt{y} \tag{34}$$

Here y is an another random variable uniformly distributed in the range 0 to 1.

5. Now we should check, if the burst in a selected position can be observed: $p_\infty(z, \chi, \omega_2, \omega_3) > p_{\min}$. If it is, add $\kappa(z, \chi)$ to the sample. If not, repeat from the step 3.

6. If the sample is not as big as we want yet, repeat from the step 3.

With this algorithm, we arrive to our second test / constraint for the burst parameters. The obtained stretching factors distribution should be compatible with observations.

3.8 High energy bursts fraction

Out final test is the comparison of answers to this question: given the bursts which were observed in a whole energy range (ω_1, ω_3), which fraction of them can also be observed in a high energy range (ω_2, ω_3)?

To calculate this value, we need to compute the number of bursts visible in a given energy range, which is the integral over space and jet directions:

$$\begin{aligned} b(\omega_1, \omega_2) &= \int_0^{z_{\max}(\omega_1,\omega_2)} \mathrm{d}V(z)\,\rho(z) \int_0^{\chi_{\max}(z,\omega_1,\omega_2)} 2\pi \sin\chi \,\mathrm{d}\chi \\ &\approx 2\pi \int_0^{z_{\max}(\omega_1,\omega_2)} \mathrm{d}V(z)\,\rho(z) \int_0^{\chi_{\max}(z,\omega_1,\omega_2)} \chi \,\mathrm{d}\chi = \pi \int_0^{z_{\max}(\omega_1,\omega_2)} \mathrm{d}V(z)\,\rho(z)\,\chi^2_{\max}(z, \omega_1, \omega_2) \end{aligned} \tag{35}$$

Here $z_{\max}(\omega_1, \omega_2)$ and $\chi_{\max}(z, \omega_1, \omega_2)$ are the same values we used in the previous section: the maximum redshift from which a burst can be observed in a given energy range, and the maximum off-axis angle with which the burst at redshift z can be observed.

The fraction we want to compute is the ratio of these integrals:

$$f(\omega_1, \omega_2, \omega_3) = \frac{b(\omega_2, \omega_3)}{b(\omega_1, \omega_3)} = \frac{\int_0^{z_{\max}(\omega_2,\omega_3)} \mathrm{d}V(z)\,\rho(z)\,\chi^2_{\max}(z, \omega_2, \omega_3)}{\int_0^{z_{\max}(\omega_1,\omega_3)} \mathrm{d}V(z)\,\rho(z)\,\chi^2_{\max}(z, \omega_1, \omega_3)} \tag{36}$$

This is our 3rd test – the ratio obtained should be compatible with the observed value.

3.9 Parameter values

Finally, we are in a position to use the tests to fit parameters of the model.

- v, the velocity of the shell, $\gamma = \frac{1}{\sqrt{1-v^2}} \gg 1$.
- η_0, which defines the luminosity scale.
- r_0, the characteristic jet length; $r_0 \ll \frac{1}{H(0)}$, $H(t)$ is the Hubble parameter;

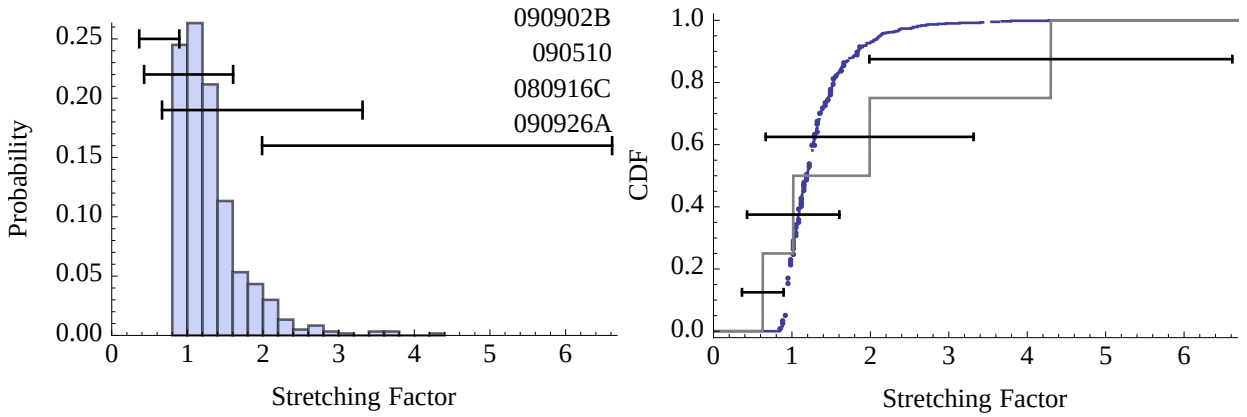

Figure 7: The histogram and the CDF of the stretching factors sample produced by our model (blue). The sample contains 600 points. The gray curve is an empirical CDF of the observed sample (4 points).

- n, which determines the sharpness of the jet end, $n > 3$;
- ω_0, a characteristic radiation frequency;
- θ_0, the opening angle of the jet for radiation with frequency ω_0, $\theta_0 \ll 1$;
- k, which determines how much the opening angle changes with frequency, $k < 0$;
- α, the bare spectral index, $\alpha < -2k - 1$

3.10 Results

4 Discussion

References

[AAA+13] M. Ackermann, M. Ajello, K. Asano, M. Axelsson, L. Baldini et al., *The First Fermi-LAT Gamma-Ray Burst Catalog*, Astrophys.J.Suppl. **209**, 11 (2013), 1303.2908.

[BFK03] J. S. Bloom, D. Frail and S. Kulkarni, *GRB energetics and the GRB Hubble diagram: Promises and limitations*, Astrophys.J. **594**, 674–683 (2003), astro-ph/0302210.

[Fermi-LAT12] M. Ackermann et al. (Fermi-LAT Collaboration), *The Fermi Large Area Telescope On Orbit: Event Classification, Instrument Response Functions, and Calibration*, Astrophys.J.Suppl. **203**, 4 (2012), 1206.1896.

[Fermi11] M. Ackermann et al. (Fermi Collaboration), *Detection of a spectral break in the extra hard component of GRB 090926A*, Astrophys.J. **729**, 114 (2011), 1101.2082.

[FLG09] H. Tajima (Fermi-LAT and GBM Collaborations), *Fermi Observations of high-energy gamma-ray emissions from GRB 080916C*, (2009), 0907.0714.

[FS09] A. Abdo et al. (Fermi/GBM, Fermi/LAT and Swift Collaborations), *Fermi Observations of GRB 090902B: A Distinct Spectral Component in the Prompt and Delayed Emission*, Astrophys.J. **706**, L138–L144 (2009), 0909.2470.

[GR13] N. Gehrels and S. Razzaque, *Gamma Ray Bursts in the Swift-Fermi Era*, Front.Phys.China. **8**, 661–678 (2013), 1301.0840.

[LP13] J. Lange and M. Pohl, *The average GeV-band Emission from Gamma-Ray Bursts*, (2013), 1301.2914.

[NI01] T. Nakamura and K. Ioka, *Peak luminosity-spectral lag relation caused by the viewing angle of the collimated gamma-ray bursts*, (2001), astro-ph/0105321.

[RPT12] G. Rubtsov, M. Pshirkov and P. Tinyakov, *GRB observations by Fermi LAT revisited: new candidates found*, Mon.Not.Roy.Astron.Soc.Lett. **421**, L14–L18 (2012), 1104.5476.

[Science04] N. Gehrels et al. (Swift Science Collaboration), *The Swift Gamma-Ray Burst Mission*, AIP Conf.Proc. **727**, 637–641 (2004), astro-ph/0405233.

[SSD+13] A. Shenoy, E. Sonbas, C. Dermer, L. Maximon, K. Dhuga et al., *Probing Curvature Effects in the Fermi GRB 110920*, Astrophys.J. **778**, 3 (2013), 1304.4168.

[SSL05] R.-F. Shen, L.-M. Song and Z. Li, *Spectral lags and the energy dependence of pulse width in gamma-ray bursts: Contributions from the relativistic curvature effect*, Mon.Not.Roy.Astron.Soc. **362**, 59–65 (2005), astro-ph/0505276.

[Via13] G. Vianello, *Observations of Gamma-ray Bursts in the Fermi era*, (2013), 1304.5570.

[YLQL06] T.-F. Yi, E.-W. Liang, Y.-P. Qin and R.-J. Lu, *On the spectral lags of the short gamma-ray bursts*, Mon.Not.Roy.Astron.Soc. **367**, 1751–1756 (2006), astro-ph/0512270.